Modeling the Performance of Single-Bit and Multi-Bit Quanta Image Sensors

Eric R. Fossum, *Fellow, IEEE*

***Abstract*—Imaging performance metrics of single-bit and multi-bit photo-electron-counting quanta image sensors (QIS) are analyzed using Poisson arrival statistics. Signal and noise as a function of exposure are determined. The D-log H characteristic of single-bit sensors including overexposure latitude is quantified. Linearity and dynamic range are also investigated. Read-noise-induced bit-error rate is analyzed and a read-noise target of less than 0.15 e-rms is suggested.**

***Index Terms*—Active pixel sensor, APS, binary pixel, CIS, CMOS image sensor, low noise, multi-bit pixel, photon counting, photoelectron counting, Poisson statistics, QIS, quanta image sensor.**

I. Introduction

SOLID-STATE image sensors, such as the charge-coupled device (CCD) or CMOS active pixel image sensor (CMOS APS or CIS), have an array of photodetectors that convert photons to photoelectrons (or photoholes) and collect those carriers in an electrostatic potential well. After some integration period, carriers are read out as a voltage signal via some conversion gain (CG) usually determined by a combination of the capacitance of the readout node and signal chain amplification factor. The voltage signal is subsequently converted from analog to digital format. Each photodetector corresponds to a pixel. The pixel has a maximum signal, usually called "full well," measured in electrons. Due to photon shot noise, the maximum signal-to-noise ratio (SNR) achievable by the pixel is the square root of this value. The dynamic range (DR) of the pixel is defined as the ratio of the maximum light signal that can be accommodated by the image sensor pixel (often limited by the full well size) to that of the light-referred noise in the dark. Most image sensors are designed for linear response to light, but some high dynamic range (HDR) sensors compand the signal by various means to increase the maximum light signal that can be accommodated.

The Quanta Image Sensor (QIS) was conceived in 2004 while considering the consequences and limits of pixel shrink in consumer-electronics image sensors [1]. One consequence of pixel shrink is reduction in SNR and image quality caused by the reduction in full well capacity. To mitigate this problem a new type of image sensor paradigm was proposed [2], now referred to as the QIS [3]. In this paradigm, very small pixels (e.g. 100–200 nm pitch) with intentionally small full well capacity (e.g., 1–200 carriers) are used to oversample the image in spatial and time domains. Signal processing is then applied to the acquired spatial-temporal data cube to produce image pixels. Oversampling, in various forms, is now considered one of the pathways for future image sensor development [4]–[6].

The single-bit QIS is nominally organized as an array of photodetectors each sensitive to a single photoelectron. While in practice the photodetector may continue to be sensitive to multiple photoelectrons, subsequent circuitry discriminates the output to one of two binary states: either a "0" meaning no photoelectron, or a "1" meaning at least one photoelectron. These highly specialized photodetectors are referred to as "jots" from the Greek word meaning "smallest thing." Small jot pitches are needed more for storage capacity (photoelectrons/cm^2) than for increased optical resolution. A QIS image sensor for consumer use is expected to contain 100Mjots-10Gjots. As an example, a 42k $\times$ 24k 200 nm jot-pitch QIS would have 1 Gjots with a 10 mm image diagonal. The QIS might be readout at several hundred fields per second. Many captured fields are read out and processed to form a single image frame. A pixel in the final image may be formed from thousands of jots, such as a spatio-temporal kernel of $16\times16\times16$ jots, and the number of output image pixels is independent of the number of jots in the sensor. We have recently reported progress on image formation algorithms, jot device concepts, and readout circuit design. For example, power dissipation for a 1 Gjot QIS at 1000 fields per second (1 Tb/s) internal readout using a 22 nm process was estimated to be 880 mW [7].

Unlike conventional image sensors, where the output image pixel size is typically defined by the physical dimensions of the semiconductor pixel structure, in the QIS the final output pixel size is programmable and can be dynamically adjusted to trade resolution for sensitivity, for example, by increasing the spatio-temporal kernel size to capture more signal. Furthermore, sequential fields can be shifted from one another to permit deblurring from relative object motion and allowing a sort of noiseless time-delay and integration mode to be implemented for tracking and imaging objects under low light. Such functionality extends the application space of the QIS beyond consumer electronics.

Manuscript received May 16, 2013; revised July 24, 2013; accepted August 22, 2013. Date of publication September 30, 2013; date of current version December 24, 2013. This work was sponsored in part by Rambus, Inc. The review of this paper was arranged by Editor A. G. Unil Perera.

The author is with the Thayer School of Engineering at Dartmouth, Hanover, NH 03755 USA (e-mail: eric.r.fossum@dartmouth.edu).

Color versions of one or more of the figures in this paper are available online at http://ieeexplore.ieee.org.

Digital Object Identifier 10.1109/JEDS.2013.2284054

Also considered in this work are multi-bit photoelectron-counting sensors. An example of this type of sensor is the quantized digital integration sensor (qDIS)—a sort of multi-bit QIS [4]. For a multi-bit photoelectron counting sensor, it is desired that each pixel is read out and converted to a digital value corresponding to the number of photoelectrons in the pixel. In the multi-bit QIS the full well capacity is relatively small (e.g., 3 to 127 e-) and multiple fields are digitally integrated to form the image. The advantage of the multi-bit QIS is, of course, storage capacity density. For example, using a 3-bit pixel one can store up to 7 electrons with little impact on pixel design. The trade-off between single-bit and multi-bit systems for the same pixel size and dynamic range is higher readout rates and simpler and lower power ADC for the single-bit system compared to lower readout rates and more complicated, higher power ADC for the multi-bit system.

The QIS belongs to a broad class of sensors that could be called photon-counting or photoelectron-counting sensors but most prior work on photon-counting sensors has focused on low resolution, low light scientific imaging [8]. Single-photon avalanche-detectors (SPADs) [9]–[11] are near-miss candidate devices for the QIS jot because they are relatively large area devices (due in part to the large electric fields required for avalanche) with relatively low spatial resolution (thousands of pixels) and often are often operated in asynchronous or event-driven readout mode. High-energy-photon-counting sensors have also been developed where many photoelectrons are generated by a single x-ray photon, but these devices are not applicable to general consumer imaging due to the imaging wavelengths and also have low spatial resolution, large pixels [e.g., 12] and most importantly, operate under sparse exposure conditions.

Analysis using Poisson arrival statistics helps reveal the imaging performance characteristics of the QIS under all exposure conditions. Yang, et al., reported on reconstructing images with binary-pixel sensors and applied photon statistics [13]. Teranishi recently reported the application of photon statistics to photon-counting in image sensors to estimate quantum efficiency and read noise requirements [14].

This work amplifies and extends those analyses to conventional and important imaging performance metrics such as linearity, noise, and dynamic range for single-bit and multi-bit QIS devices. Predicting the imaging performance of the QIS is important to do prior to investing significant effort to further develop this type of sensor.

II. Signal

Photons are emitted from light sources at some average rate on longer time scales, but stochastically on shorter time scales, and their emission from most light sources is well-described by the Poisson process. Through various attenuating and reflective processes, the photons arrive at a photodetector where they are absorbed and converted to photoelectrons and collected with some quantum efficiency (QE). Both the photon stream entering the photodetector and the photoelectrons collected by the photodetector are described by the Poisson process. This means that the average number of arrivals over some time interval τ depends only on the average arrival rate $\bar{\phi}$ (e.g., photoelectrons per second per photodetector) and the length of the interval τ, and in fact, just on the product $\bar{\phi}\tau$ that will be called the *quanta exposure* H. A quanta exposure of H means H photons or photoelectrons arrive at the photodetector on average over the interval τ. The number of photons arriving in sequential intervals for H = 1 is illustrated in Fig. 1.

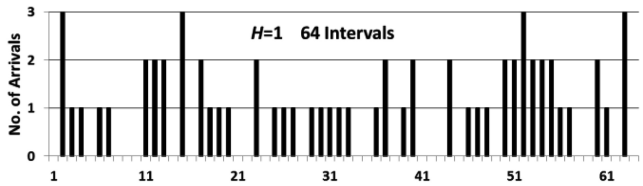

Fig. 1. A Monte-Carlo simulation of arrivals per time interval is shown for H = 1 for 64 intervals. It is seen that many intervals have multiple arrivals and some have no arrivals.

In the Poisson process [15], the probability $P[k]$ of k arrivals for exposure H is given by:

$$P[k] = \frac{e^{-H}H^k}{k!} \tag{1}$$

Thus, the probability of no arrivals ($k = 0$) is:

$$P[0] = e^{-H} \tag{2}$$

The probability of at least one arrival ($k > 0$) is simply given by:

$$P[k>0] = 1 - P[0] = 1 - e^{-H} \tag{3}$$

A. Signal in Single-Bit Pixels

In the QIS, each jot has an integration period τ during which one or more photoelectrons might be collected. After the end of the integration period, the state of the jot is read out. It is then reset and the process starts again, typically with the same integration period τ. Note that the integration period τ could be less than the time between readouts since the jot could be reset at some time between readout cycles.

Let the jot have just two states at the end of the integration period, J_0 or J_1, corresponding respectively to the absence or presence of at least one photoelectron. The probabilities of these states $P[J_0]$ and $P[J_1]$ are given by (2) and (3) respectively. The single-bit QIS jot has a full well capacity FW of one electron. It is assumed that a full jot does not bloom into a neighboring empty jot—if it does, it could substantially change this analysis.

In an ensemble of M jots uniformly illuminated, let the expected number of jots in state J_0 be given by M_0:

$$M_0 = M \cdot P[J_0] = Me^{-H} \tag{4}$$

and the expected number of jots in state J_1 be given by M_1:

$$M_1 = M \cdot P[J_1] = M \cdot \left[1 - e^{-H}\right] \tag{5}$$

Let the *bit density*, D be defined as:

$$D \triangleq \frac{M_1}{M} = P[J_1] \tag{6}$$

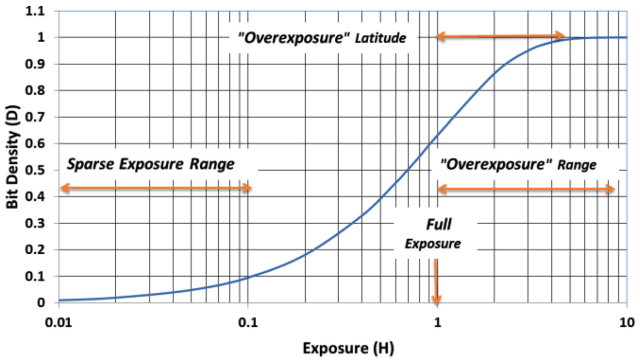

Fig. 2. D-logH exposure characteristic of the Quanta Image Sensor.

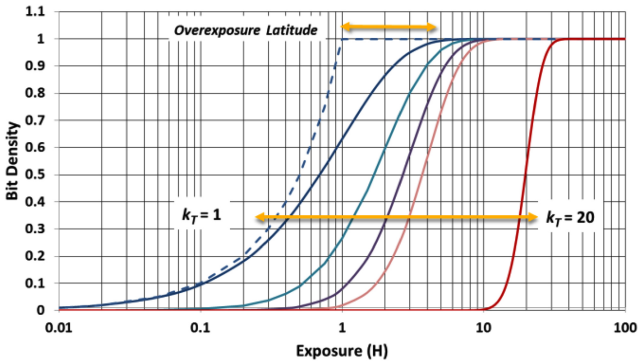

Fig. 3. Bit density vs. log exposure for pixel requiring multiple carriers to change state, for thresholds k_T of 1, 2, 3, 4 and 20 photoelectrons. Also shown is a simple linear response and the overexposure latitude.

For *sparse exposure*, defined as $H \lesssim 0.1$, the bit density is given by the linear relationship:

$$D \cong H \tag{7}$$

The non-linearity NL of the bit density vs. exposure can be measured as the fractional deviation from linear response above in (7) extrapolated to higher exposures.

$$NL \triangleq \frac{MH - M_1}{MH} \cong \frac{H}{2} - \frac{H^2}{6} \tag{8}$$

for the range $0 \leq H \lesssim 1$ so that 5% non-linearity is reached at approximately $H = 0.1$.

At "*full exposure*" ($H = FW = 1$) bit density is just 63%. At 2x overexposure ($H = 2FW$), it is 86%, and at 5x overexposure ($H = 5FW$) the bit density reaches 99.3%. The *overexposure latitude* is defined in this paper as the ratio of the exposure where the bit density achieves 99% of its maximum value to the full exposure. The overexposure latitude for the QIS is easily calculated from (5) as 4.6x. Bit density is shown in Fig. 2 as a function exposure. The exposure H can be recovered in the non-linear ranges by using (5) and the measured bit density.

As was discussed qualitatively in [2] this D-log H "S-shaped curve" is quite similar to the famous D-log H plot for photographic plate densities following light exposure and development, as reported by Hurter and Driffield in 1890 [16]. The curve means that film response is non-linear and can tolerate highlights much better than a conventional solid-state image sensor—a feature highly desired by classic photographers and cinematographers. Thus, the analogous performance of the QIS may be of interest for those applications. For conventional sensors some of this non-linear response can be encoded in the postprocessing of the linear-response image. Nevertheless, the non-linear response of film has been hard to match even in HDR solid-state image sensors without introducing artifacts due to motion, threshold voltage fixed-pattern variation, and other circuit design issues [17], [18]. For the QIS, the non-linear response is determined by its fundamental operating characteristics.

B. Signal in Multi-Carrier Single-Bit Pixels

In film it often takes multiple photons to result in the exposure of a single grain [19]. In a solid-state analog of that process, the output of a single-bit pixel would be "0" if the number of photoelectrons k was less than a threshold k_T. Thus the probability of a multi-carrier single-bit pixel being in state J_0 is:

$$P[J_0] = \sum_{k=0}^{k_T-1} P[k] \tag{9}$$

And the probability of being in state J_1 is:

$$P[J_1] = 1 - P[J_0] \tag{10}$$

Bit density D as a function of exposure is shown below Fig. 3 for a variety of thresholds. It is seen that the overexposure latitude reduces for an increase in multi-carrier threshold.

C. Signal in Multi-Bit Pixels

In an n bit multi-bit photoelectron-counting image sensor let the full well capacity of the pixel be given by FW where:

$$FW = 2^n - 1 \tag{11}$$

which may be between, say, $2^2 - 1 = 3$ and $2^8 - 1 = 127$ electrons for a 2-bit and 8-bit multi-bit sensor respectively. The full well might be limited by carrier storage capacity in the pixel, but more likely by the analog-to-digital converter (ADC) resolution, so that signals greater than FW are clipped by the ADC.

For an exposure H the probability that a pixel contains k photoelectrons $P[k]$ is given by (1) so that the expected number of photoelectrons $<k>$ stored in a pixel with full well FW is given by:

$$<k> = \sum_{k=0}^{FW} k \cdot P[k] + \sum_{k=FW+1}^{\infty} FW \cdot P[k] \tag{12}$$

In an ensemble of M equally illuminated pixels (say, one pixel read over multiple fields), the total sum of expected pixel values is $M<k>$. This sum is shown as a function of exposure for reading 256 4-bit pixels ($FW = 15$) in Fig. 4 below. The small full-well saturation leads to a non-linear response and rounding near the transition point. Full exposure for this example is $H = FW = 15$. However, the overexposure latitude is quite small—about 1.4x in this case—compared to that of the QIS with $FW = 1$ which has a latitude of 4.6x.

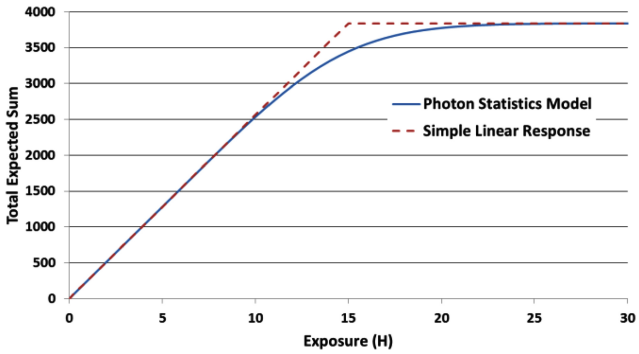

Fig. 4. Response of a multi-bit pixel (256 4b pixels are summed).

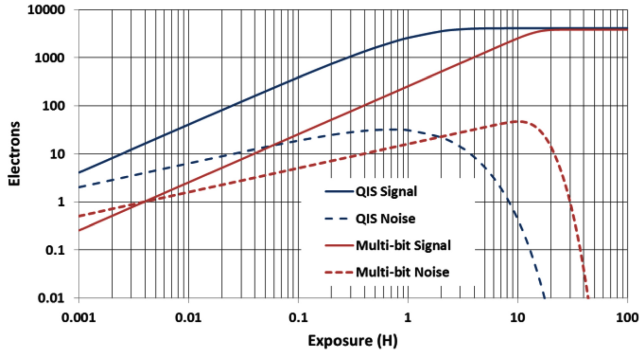

Fig. 5. Signal and noise as a function of exposure for a single-bit QIS sensor and for a multi-bit digital integration sensor. For the QIS, the signal is the sum over 4096 jots (e.g. 16×16×16). For the multi-bit sensor, the signal is the sum over 256 reads of a 4b pixel.

III. Noise

Noise in image sensors consists of fixed pattern (spatial) noise (FPN) and temporal noise. FPN can arise from variations in pixel and ADC circuit manufacturing (e.g. implantation and lithography) as well as "frozen" temporal noise due to sensor timing. In this work we only consider temporal noise.

Temporal noise in the QIS—that is, the root-mean-square (rms) variation in output from field to field for the same exposure—has three general components. The first is from the photon shot noise as reflected by Poisson statistics. The second is read noise arising during the readout process. The third is noise from dark current. The output for the QIS depends on the signal processing, but for simplicity it is assumed to be the sum over M jots. Similarly, the output for a multi-bit sensor could be the sum of the signals from M pixels, or the digitally integrated signal of one pixel from M reads or some combination of the two.

A. Photon Shot Noise in the QIS

In a conventional image sensor, where the number of signal photoelectrons is S, the variance in S due to photon shot noise is equal to S. To determine the variance σ_1^2 of the QIS signal M_1, the variance of a binomial distribution needs to be used to estimate the effect of photon shot noise since there are only two possible states. Thus one has:

$$\sigma_1^2 = M \cdot P[J_0] \cdot P[J_1] \tag{13}$$

or

$$\sigma_1^2 = \frac{M_0 M_1}{M} = M \cdot D(1-D) \tag{14}$$

which applies to single-bit pixels—both the QIS and the multi-carrier pixels. Since $M = M_0 + M_1$, one can also write:

$$\frac{1}{\sigma_1^2} = \frac{1}{M_0} + \frac{1}{M_1} \tag{15}$$

Using (4) and (5) with (13) one obtains for the QIS:

$$\sigma_1^2 = M \cdot e^{-H}\left[1 - e^{-H}\right] \tag{16}$$

Under sparse exposures, where $M_1 \ll M_0$, one has $\sigma_1^2 \cong M_1$ just as for conventional image sensors. For larger exposures, the noise is essentially "squeezed" since the number of empty jots is small and only these can contribute to a variance in M_1. Signal and noise for the QIS are plotted below in Fig. 5. It can be seen that the noise is suppressed as the illumination approaches full exposure conditions and diminishes quickly for overexposure.

The noise has a maximum value of:

$$\sigma_{1max} = \frac{1}{2}\sqrt{M} \tag{17}$$

which occurs at an exposure of $H = \ln 2$ corresponding to the jots being half filled ($M_0 = M_1 = M/2$). The noise is already squeezed at this exposure by a factor of $\sqrt{2}$ from what it would be if one just used the classical shot noise equation.

B. Photon Shot Noise in Multi-Bit Sensors

For a multi-bit sensor with M pixel samples summed, the variance is calculated according to:

$$\sigma^2 = M(<k^2> - <k>^2) \tag{18}$$

where $<k^2>$ is given by:

$$<k^2> = \sum_{k=0}^{FW} k^2 \cdot P[k] + \sum_{k=FW+1}^{\infty} FW^2 \cdot P[k] \tag{19}$$

The noise in the output of M samples is then:

$$\sigma = \sqrt{M\left(<k^2> - <k>^2\right)} \tag{20}$$

Equation (20) reduces to (16) in the case $FW = 1$. The calculated signal and noise for a 4b multi-bit sensor with $M = 256$ and $FW = 15$ is also shown in Fig. 5. For low exposures compared to full well, the noise follows the classic square-root shot-noise relationship, but like the QIS, as the probability that the storage well is full approaches unity, the noise drops.

It is interesting to compare the signal and noise curves for the single-bit and multi-bit sensors. The single photoelectron full well of the single-bit sensor leads to a more rounded transition between linear response and saturation compared to that of the relatively larger full-well multi-bit sensor, and the noise roll-off of the single-bit sensor is more gradual than that of the multi-bit sensor as well. A semi-log (e.g. D-log H) plot of the signal as a function of exposure for 1b QIS and 2b, 3b, 4b, 5b and 6b full well multi-bit sensors is shown in

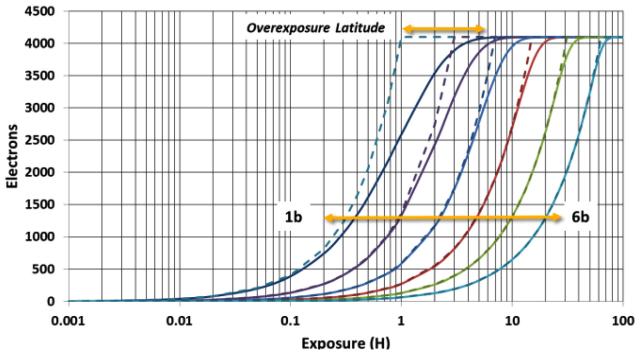

Fig. 6. Semi-log plot of signal vs. exposure for multi-bit sensors with 1b to 6b full well capacity. Also shown in dashed lines are simple linear responses. The difference in saturation exposure between the simple linear response and the calculated response illustrates the variation in overexposure latitude with full well capacity.

Fig. 6. The number of samples is adjusted for each case so that the total number of photoelectrons counted is the same. One can deduce that the capacity of the full well determines the overexposure latitude and D-log H characteristics of the sensor.

C. Read Noise for Single-Bit Sensors

During readout, the signal from the jot is both amplified and corrupted by noise. Let the uncorrupted voltage signal from the jot be given by V_{sig} with $V_{sig} = 0$ for no photoelectrons, and positive for a photoelectron. Let CG be the conversion gain (V/e-) for the signal. At a given readout rate and timing, let the rms voltage noise after readout and before analog-to-digital quantization (1b ADC for the jot) be given by V_n. It is convenient to normalize the voltage signal to the number of electrons, so let the normalized uncorrupted signal U_{sig} be defined by:

$$U_{sig} \triangleq \frac{V_{sig}}{CG} \tag{21}$$

Thus, for a jot, U_{sig} is either 0 or 1. Similarly, let the normalized noise U_n be defined by:

$$U_n \triangleq \frac{V_n}{CG} \tag{22}$$

If the read noise is described as a Gaussian distribution, then the probability $P[U]$ of reading the continuously-valued corrupted signal U is given by the normal distribution:

$$P[U] = \frac{1}{U_n\sqrt{2\pi}} exp\left[-\frac{(U-U_{sig})^2}{2U_n^2}\right] \tag{23}$$

For the jot there are two possible distributions corresponding to U_{sig} being either 0 or 1. Following the readout of the signal, U is quantized by a 1b ADC to value B. The ADC can be considered as a simple comparator with quantizer threshold U_{th} set at $U_{th} = 0.5$. The rate of bit-flip errors that are made (bit error rate, BER) as a function of the noise in the readout signal chain can determined as illustrated in Fig. 7 below.

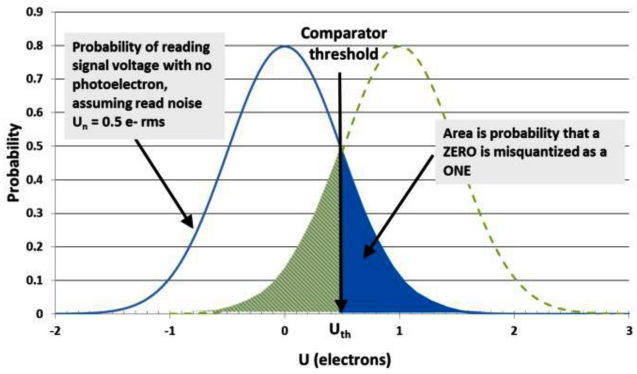

Fig. 7. Probability distribution for reading signal U for $U_{sig} = 0$ and 1. BER is determined from area under curve as shown.

The probability of $U_{sig} = 0$ being misquantized as $B = 1$ (a false positive) is given by the area under the curve shown in blue. The probability of a false positive, P_{fp} is just:

$$P_{fp} = \int_{U_{th}}^{\infty} P[U]\,dU \tag{24}$$

or

$$P_{fp} = \frac{1}{2} - \int_{0}^{U_{th}} P[U]\,dU \tag{25}$$

Performing the integral yields:

$$P_{fp} = \frac{1}{2} erfc\left[\frac{U_{th}}{\sqrt{2}U_n}\right] \tag{26}$$

And when the threshold is set in the middle, $U_{th} = 0.5$, one obtains:

$$P_{fp} = \frac{1}{2} erfc\left[\frac{1}{\sqrt{8}U_n}\right] \tag{27}$$

Similarly the probability of $U_{sig} = 1$ being quantized as $B = 0$ (a false negative) is given by the area under the curve shown in green hatch. The area is given by:

$$P_{fn} = \frac{1}{2} erfc\left[\frac{1-U_{th}}{\sqrt{2}U_n}\right] \tag{28}$$

And when $U_{th} = 0.5$ one obtains:

$$P_{fn} = \frac{1}{2} erfc\left[\frac{1}{\sqrt{8}U_n}\right] \tag{29}$$

Consider a population of M bits output from the array. The expected total number of false positives M_{fp} is given by:

$$M_{fp} = M_0 P_{fp} \tag{30}$$

And the expected total number of false negatives M_{fn} is given by:

$$M_{fn} = M_1 P_{fn} \tag{31}$$

The expected total number of bit errors is given by:

$$M_{fp} + M_{fn} = M_0 P_{fp} + M_1 P_{fn} \tag{32}$$

With $U_{th} = 0.5$ then $P_{fp} = P_{fn}$ and the total number of bit errors is given by:

$$M_{fp} + M_{fn} = \frac{M}{2} erfc\left[\frac{1}{\sqrt{8}U_n}\right] \tag{33}$$

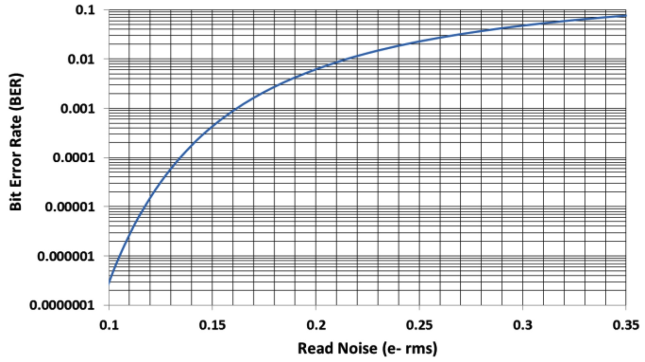

Fig. 8. BER as a function of read noise for the QIS.

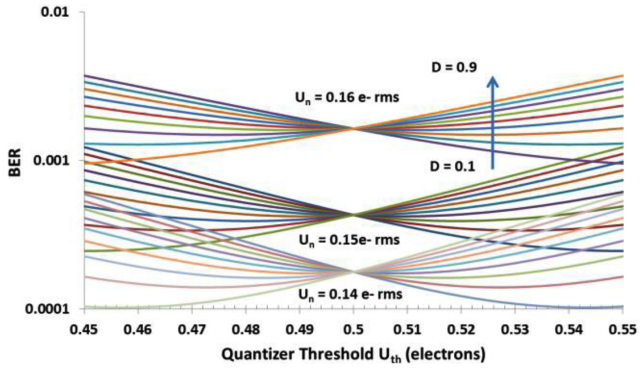

Fig. 9. Semi-log plot illustration effect of quantizer threshold on BER for different average bit densities and read noise levels.

The bit error rate BER is given by $(M_{fp} + M_{fn})/M$ or:

$$BER = \frac{1}{2} erfc \left[\frac{1}{\sqrt{8} U_n} \right] \tag{34}$$

BER as a function of read noise is shown in Fig. 8.

From Fig. 8, it is seen that BER is a steep function of read noise. Choosing a read noise value of 0.15 e- rms yields a BER that is negligible except for very sparse exposures. However, doubling the value of the read noise to 0.30 e- rms gives an unacceptable BER for nearly all exposures. On the other hand, reducing the read noise much below 0.15 e- rms has little practical effect on BER since it only becomes more negligible. Essentially then, read noise will either be a big problem or no problem in photoelectron counting sensors.

The threshold level U_{th} could be adjusted, say, more positive, if more 0's than 1's are expected, reducing the number of "false positives" [20]. It is readily apparent from (32) that if $M_0 \gg M_1$ such as occurs under sparse exposure, then minimization of the expected total number of bit errors can be achieved with $U_{th} > 0.5$. For example, if $H = 0.1$ for all jots in the array and read noise $U_n = 0.15$ e- rms, an optimal setting of $U_{th} = 0.55$ is found by numerical methods and results in a 43% reduction in bit errors on average. (However, the same BER improvement can be obtained with less than 0.01 e- rms improvement in read noise.) With higher read noise it was found that a larger adjustment in U_{th} was required for optimization. Generally, the efficacy of optimizing the quantizer threshold is low since optimization depends on bit density and would be difficult to set globally for normal or high dynamic range scenes.

The effect of quantizer threshold on BER was briefly investigated as illustrated below in Fig. 9. The strong impact of read noise dominates the effect of quantizer threshold variation on BER.

D. Read Noise for Multi-Bit Sensors

Generally, the read noise on a column in the sensor is independent of the ADC resolution at the bottom of the column, although dependent on the sampling rate. Thus the read noise for single-bit and multi-bit sensors is nominally the same, and the read-noise requirement for counting photoelectrons also the same.

Consider a pixel contains k photoelectrons that produce a uncorrupted signal of $U_{sig} = k$. After the readout signal chain,

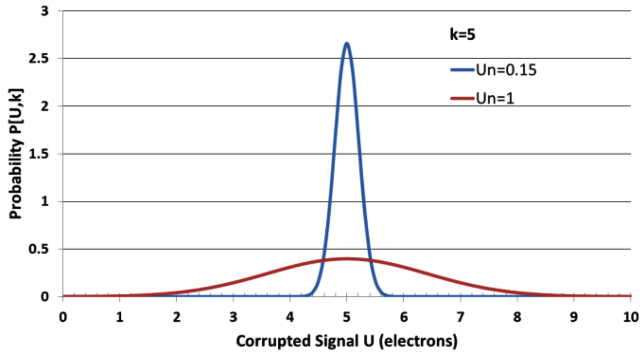

Fig. 10. Effect of read noise on signal distribution.

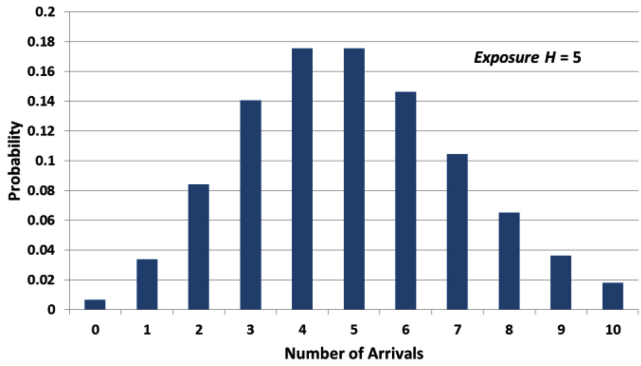

Fig. 11. Probability of having k photoelectrons in a pixel for an exposure of H = 5.

the probability of reading the corrupted signal U, assuming Gaussian noise properties is given by:

$$P[U,k] = \frac{1}{U_n \sqrt{2\pi}} exp \left[-\frac{(U-k)^2}{2U_n^2} \right] \tag{35}$$

P[U,k] is illustrated below in Fig. 10 for $k = 5$ and two cases: $U_n = 1.0$ e- rms and 0.15 e- rms.

The probability of having k photoelectrons in a pixel for quanta exposure H is given by (1) and illustrated below in Fig. 11 for the case of $H = 5$.

The product $P[U,k] \cdot P[k]$ gives the probability of reading voltage signal U due to k photoelectrons for an exposure H and is shown in Fig. 12 for two cases: $U_n = 1.0$ e- rms and 0.15 e- rms. If the signal U is quantized by setting conversion

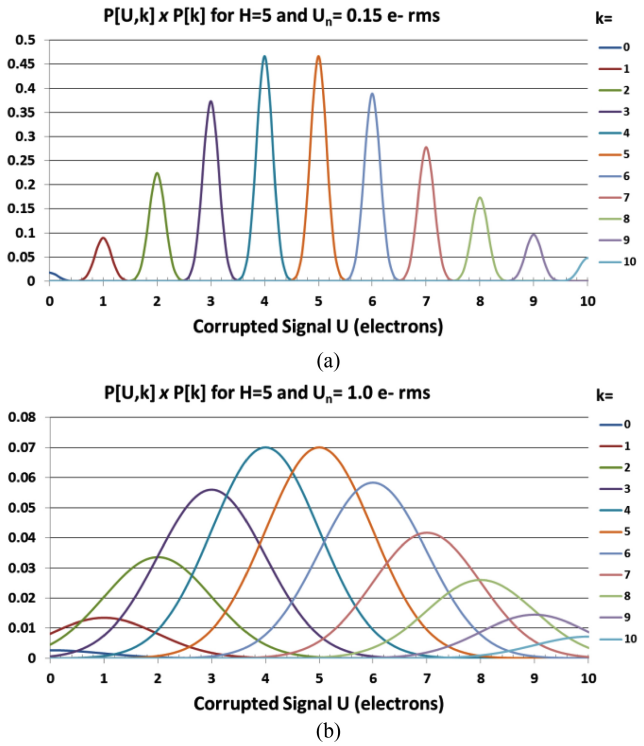

Fig. 12. Distribution of probability function product for two levels of read noise (a) 0.15 e- rms (b) 1.0 e- rms.

thresholds at the halfway point between integer values of U, it is readily apparent from Fig. 12(a) that a result of, say, 3, is highly likely to be due to a photoelectron count of 3 and no other in the case of $U_n = 0.15$ e- rms, whereas as seen in Fig. 12(b) for $U_n = 1.0$ e- rms, a result of 3 could come from $k = 3$, but almost as likely from $k = 4$, and then in decreasing likelihood, from $k = 2$, $k = 5$, $k = 1$, $k = 6$, etc. Thus to count photoelectrons, it is desired that the product $P[U, k] \cdot P[k]$ to be as large as possible for $U = k$ and negligible for $U \neq k$.

The probability that the readout of a pixel yields voltage U after exposure H is then given by summing the signal at some value U from each possible number k of photoelectrons, whose read noise is spread out over U:

$$P[U] = \sum_{k=0}^{\infty} P[U, k] \cdot P[k] \tag{36}$$

or

$$P[U] = \sum_{k=0}^{\infty} \frac{1}{U_n \sqrt{2\pi}} exp\left[-\frac{(U-k)^2}{2U_n^2}\right] \cdot \frac{e^{-H} H^k}{k!} \tag{37}$$

P[U] is shown below in Fig. 13 for $U_n = 0.15$ e- rms and for $U_n = 1.0$ e- rms. From the figure one can see that it should be easy to quantize and count photoelectrons for low read noise but for higher noise it is impossible. It is noted that the peak of the noisier distribution is for $U = 4.5$, reflective of $P[k = H] = P[k = H - 1]$.

The two-dimensional signal histogram in Fig. 14 shows the probability of reading signal U_{sig} for different exposure levels with read noise fixed at 0.15 e- rms.

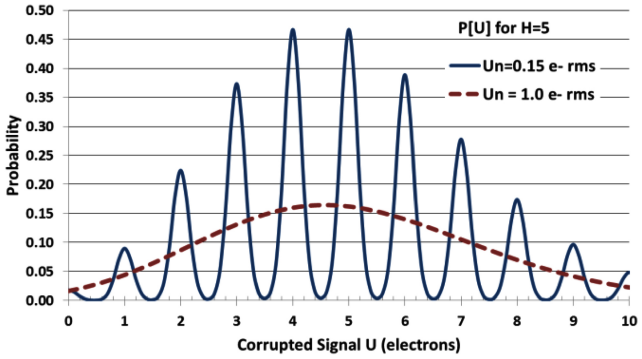

Fig. 13. Probability distribution for reading corrupted signal U for two different levels of read noise, 0.15 e- rms and 1.0 e- rms for an exposure H = 5.

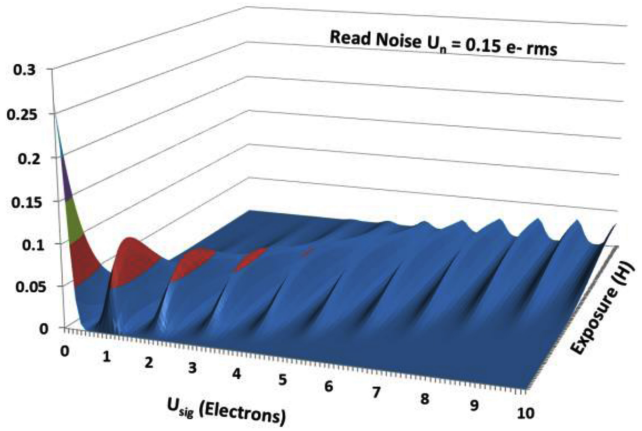

Fig. 14. A two-dimensional signal histogram as a function of exposure (H = 0 to 10) for read noise of 0.15 e-rms.

In an ensemble of M pixels, the number of pixels with value U is just $M \cdot P[U]$. The total number of photoelectrons N in the ensemble is then estimated to be:

$$N = M \int_0^{\infty} U \cdot P[U]\, dU \tag{38}$$

IV. QIS Signal-to-Noise Ratio

Signal to noise ratio (SNR) for the QIS can be readily calculated. The signal S is M_1. The noise is σ_1 and SNR is thus given by:

$$SNR = \sqrt{\frac{M_1}{1 - M_1/M}} \tag{39}$$

For non-linear response, exposure-referred SNR, SNR_H, is a more meaningful metric, especially because when the noise is squeezed, the voltage-referred SNR artificially rises. SNR_H can be determined according to:

$$SNR_H = \frac{H}{\sigma_H} \tag{40}$$

where the exposure-referred noise σ_H is obtained from:

$$\sigma_H = \sigma_1 \frac{dH}{dM_1} \tag{41}$$

From (5) one has:

$$\frac{dH}{dM_1} = \frac{1}{Me^{-H}} \tag{42}$$

Thus, SNR_H is given by:

$$SNR_H = \sqrt{M}\frac{H}{\sqrt{e^H - 1}} \tag{43}$$

V. Dynamic Range

Dynamic range, *DR*, is defined as ratio of maximum exposure H_m that just saturates the sensor (or less, depending on linearity requirements) and the exposure-equivalent temporal noise H_n level in the dark according to:

$$DR = 20\log\left(\frac{H_m}{H_n}\right) \tag{44}$$

For this paper, H_m is defined as the exposure where the signal reaches 99% of saturation—the same as for determining overexposure latitude. The value of H_n is determined from read noise entering the column sense amplifier and dark current counts

Let H_n consist of two components, H_{nr} for read noise and H_{nd} for dark current. Generally, one component or the other dominates. Read-noise induced false positives are indistinguishable from signal so from (26) one obtains:

$$H_{nr} = \frac{1}{2}erfc\left(\frac{1}{\sqrt{8}U_n}\right) \tag{45}$$

Dark current is difficult to predict, but generally one can expect levels similar to those in present day CMOS image sensors. Jot areas are smaller, voltages lower, but field-bunching stronger and doping higher, among other factors. For example, SOA is 15 e-/s at 60C for a 1.4 um pixel [21]. A jot that is 1/100th the area might reasonably be expected to have a dark current of 0.5 e-/s. For a 16x time-oversampled QIS, the integration interval might be 2 msec so the expected number of dark carriers is 0.001. This is 4 dark bits out of every 4096 and best considered temporal noise. An exposure-equivalent dark current H_{nd} can be assigned and set it to 0.001 in this estimate. Note H_{nd} depends on the integration time since exposure is defined as the number of expected arrivals over the integration interval.

The dynamic range for the single-bit QIS extends from the greater of H_{nr} and H_d, to $H_m = 4.6$, yielding a dynamic range of approximately 20 log (4.6/0.001) = 73 dB. For multi-bit sensors where the number of bits is about 6 or higher, $H_m \cong FW$ (see Fig. 6.) and the classic value of *DR* is obtained.

VI. QIS High Dynamic Range

As in conventional CMOS image sensors [22], dynamic range can be improved by combining different integration periods. In Fig. 5 the transfer characteristic and SNR for a QIS device was shown, where nominally the 4096 jot samples could be considered 16×16 in space, and 16 time slices, with all samples having the same integration time. In that case, the SNR peaked at about 51. Instead, just as an example, one could break the 16 time slices up into 4 groups with 4 slices each, each group having a different integration time for the time slices. For example, the first group of slices could have an integration time of 1 (normalized to the readout scan time), the 2nd 0.2, the 3rd 0.04, and the 4th 0.008—basically 5x difference between each set. The total readout time for the QIS would be the same, but the exposure period would be different for each group.

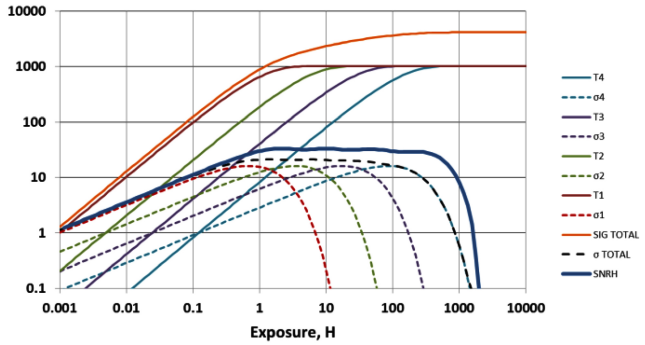

Fig. 15. Illustration of high dynamic range exposure with QIS. Maximum exposure H_m is extended about 125x or 42 dB. Exposure-referred SNR_H is relatively flat at about 30 dB. Solid lines are total bit count, dashed lines are noise in bits rms, and SNR_H has no units.

This example is illustrated in Fig. 15. The signal output from each group (assuming they are summed) is shown as a function of exposure, along with the noise as a function of exposure. The total noise is also shown. Finally, the exposure referred SNR_H is shown.

The maximum exposure has been extended to $H_m \cong 400$, an extension of 80x or 38 dB to a total *DR* of 112 dB. SNR_H is relatively flat between $H = 1$ and $H = 400$ with a value of ~30 or 30 dB, representing a drop of about -4 dB from its single integration interval peak. The flatness of the SNR is a large improvement compared the SNR dips typically found in HDR multi-integration time sensors [4].

Summing the outputs is one way of creating the HDR output signal, but other methods with improved linearity can also be considered. One example is weighting the sum of each group before summing the group signals.

Generally for HDR operation, the shape of the SNR curve and its rough value is traded against *DR* through the choices of integration intervals and number of slices in each group. Higher *DR* comes at the expense of lower *SNR*, at least over some exposure range.

VII. Conclusion

Single-bit and multi-bit image sensors have been analyzed. Linearity and overexposure latitude are found to be dependent on full-well capacity. In addition to a paradigm shift to mitigate the effects of pixel shrink and improve the flexibility of image capture, the properties of the single-bit QIS device can be exploited to yield photographic-film-like exposure properties as well as high dynamic range with nearly flat exposure-referred SNR. The read noise of single-bit and multi-bit systems has been analyzed and it is found that for photoelectron counting, read noise less than approximately 0.15 e- rms is desired. Such

accurate electron counting systems might also find application in solid-state memory devices.

ACKNOWLEDGMENTS

The author appreciates helpful discussions with Prof. M. Borsuk, Prof. K. Odame and his graduate students at Dartmouth, and Prof. Y. Lu at Harvard.

REFERENCES

[1] E. R. Fossum, "Some thoughts on future digital still cameras," in *Image Sensors Signal Processing for Digital Still Cameras*, J. Nakamura, Ed. Boca Raton, FL, USA: CRC Press, 2005, pp. 305–314.

[2] E. R. Fossum, (2005, Jun.) "What to do with sub-diffraction-limit (SDL) pixels?—A proposal for a gigapixel digital film sensor (DFS)," in *Proc. IEEE Workshop Charge-Coupled Devices Advanced Image Sensors*, [Online]. Available: http://www.imagesensors.org

[3] E. R. Fossum, "The quanta image sensor (QIS): Concepts and challenges," in *Proc. Opt. Soc. Am. Topical Meeting Comput. Opt. Sensing Imaging*, Jul. 2011.

[4] S. Chen, A. Ceballos, and E. R. Fossum, "Digital integration sensor," in *Proc. 2013 Int. Image Sensor Workshop (IISW)*, Jun. 2013.

[5] J. Alakarhu, S. Koskinen, and E. Tuulos, "Image quality of oversampling cameras," in *Proc. 2013 Int. Image Sensor Workshop (IISW)*, Jun. 2013.

[6] T. Vogelsang, M. Guidash, and S. Xue, "Overcoming the full well capacity limit: High dynamic range imaging using multi-bit temporal oversampling and conditional reset," in *Proc. 2013 Int. Image Sensor Workshop (IISW)*, Jun. 2013.

[7] S. Masoodian, Y. Song, D. Hondongwa, J. Ma, K. Odame, and E. R. Fossum, "Early research progress on quanta image sensors," in *Proc. 2013 Int. Image Sensor Workshop (IISW)*, Jun. 2013.

[8] P. Seitz and A. J. P. Theuwissen, Eds., *Single-Photon Imaging*, vol. 160. Berlin, Germany: Springer, 2011.

[9] E. Charbon, M. Fishburn, R. Walker, R. Henderson, and C. Niclass, "SPAD-based sensors," in *TOF Range Imaging Cameras*, F. Remondino and D. Stoppa, Eds. Berlin, Germany: Springer, 2013.

[10] E. Charbon, "Will avalanche photodiode arrays ever reach 1 megapixel?" in *Proc. 2007 Int. Image Sensor Workshop (IISW)*, 2007.

[11] N. Dutton, L. Grant, and R. Henderson, "9.8 μm SPAD-based analogue single photon counting pixel with bias controlled sensitivity," in *Proc. 2013 Int. Image Sensor Workshop (IISW)*, Jun. 2013.

[12] B. Dierickx, S. Vandewiele, B. Dupont, A. Defernez, N. Witvrouwen, and D. Uwaerts, "Two-color indirect X-ray photon counting image sensor," in *Proc. 2013 Int. Image Sensor Workshop (IISW)*, Jun. 2013.

[13] F. Yang, Y. M. Lu, L. Sbaiz, and M. Vetterli, "Bits from photons: Oversampled image acquisition using binary Poisson statistics," *IEEE Trans. Image Process.*, vol. 21, no. 4, pp. 1421–1436, Apr. 2012.

[14] N. Teranishi, "Required conditions for photon-counting image sensors," *IEEE Trans. Electron Devices*, vol. 59, no. 8, pp. 2199–2205, Aug. 2012.

[15] B. E. A. Saleh and M. C. Teich, *Fundamentals of Photonics*. New York, NY, USA: Wiley, 1991.

[16] Hurter and Driffield, *J. Soc. Chem. Ind.*, May 1890, reference unverified, vol. 9, pp. 455–469, May 1890.

[17] O. Yadid-Pecht, "Wide-dynamic-range sensors," *Opt. Eng.* vol. 38, no. 10, pp. 1650–1660, 1999.

[18] J. Solhusvik, J. Kuang, Z. Lin, S. Manabe, J.-H. Lyu, and H. Rhodes, "A comparison of high dynamic range CIS technologies for automotive applications," in *Proc. 2013 Int. Image Sensor Workshop (IISW)*, Jun. 2013.

[19] B. Dierickx, "Electronic image sensors vs. film: Beyond state of the art," in *Proc. OEEPE Workshop Automation Digital Photogrammetric Prod.*, Jun. 1999.

[20] Y. Lu, private communication, Apr. 2013.

[21] G. Agranov, S. Smith, R. Mauritzson, S. Chieh, U. Boettiger, X. Li, *et al.*, "Pixel continues to shrink. . . . Small pixels for novel CMOS image sensors," in *Proc. 2011 Int. Image Sensor Workshop*, Jun. 2011.

[22] O. Yadid-Pecht, C. Staller, and E. R. Fossum, "Wide intrascene dynamic range CMOS APS using dual sampling," *IEEE Trans. Electron Devices*, vol. 44, no. 10, pp. 1721–1723, Oct. 1997.

Eric R. Fossum (S'80–M'84–SM'91–F'98) was born in Connecticut, USA. He received the B.S. degree in physics and engineering from Trinity College, Hartford, CT, USA, in 1979, and the Ph.D. degree in engineering and applied science from Yale University, New Haven, CT, USA, in 1984. From 1984 to 1990, he was a Member of the Faculty of Electrical Engineering, Columbia University, New York, NY, USA. In 1990, he joined the NASA Jet Propulsion Laboratory (JPL), California Institute of Technology, Pasadena, CA, USA, and managed JPL's image sensor and focal-plane technology research and advanced development. While at JPL, he invented the CMOS active pixel sensor camera-on-a-chip technology now used in billions of camera phones, webcams, DSLRs, and other applications. In 1995, he co-founded Photobit Corporation to commercialize the technology and served in several top management roles, including Chief Executive Officer (CEO). In late 2001, Photobit Corporation was acquired by Micron Technology, Inc., Boise, ID, USA. From 2005 to 2007, he was the CEO of Siimpel Corporation, developing camera modules with MEMS-based autofocus and shutter functions for cell phones. From 2008 to 2013, he was a Consultant with Samsung Electronics focusing on various projects, including 3-D RGBZ ranging image sensors. Since 2010, he has been a Professor with the Thayer School of Engineering and Dartmouth and Faculty Coordinator of the Ph.D. Innovation Program. He has published over 260 technical papers and is the holder of more than 140 U.S. patents worldwide. He co-founded the International Image Sensor Society and served as the President until 2013. He was the Guest Editor-in-Chief for the IEEE TRANSACTIONS ON ELECTRON DEVICES special issues on solid-state image sensors in 1997, 2003, and 2009. He has received Yale's Becton Prize, the IBM Faculty Development Award, the National Science Foundation Presidential Young Investigator Award, the JPL Lew Allen Award for Excellence, the NASA Exceptional Achievement Medal, the Photographic Society of America's Progress Medal, the Royal Photographic Society's Progress Medal, and the IEEE Andrew S. Grove Award. He is a Charter Fellow of the National Academy of Inventors and is a member of the National Academy of Engineering. In 2011, he was inducted into the National Inventors Hall of Fame.